Eur. Phys. J. B **44**, 265–276 (2005)
DOI: 10.1140/epjb/e2005-00125-4

THE EUROPEAN PHYSICAL JOURNAL B

Metal-insulator transition in the quarter-filled frustrated checkerboard lattice

Y.Z. Zhang[1,a], Minh-Tien Tran[1,3], V. Yushankhai[1,4], and P. Thalmeier[2]

[1] Max-Planck-Institut für Physik komplexer Systeme, Nöthnitzer Strasse 38 01187 Dresden, Germany
[2] Max-Planck-Institut für Chemische Physik fester Stoffe, Nöthnitzer Straße 40 01187 Dresden, Germany
[3] Institute of Physics, P.O. Box 429, Bobo, 10000 Hanoi, Vietnam
[4] Joint Institute for Nuclear Research, Dubna, Russia

Received 22 November 2004
Published online 28 April 2005 –

Abstract. We study the electronic structure and correlations in the geometrically frustrated two dimensional checkerboard lattice. In the large U limit considered here we start from an extended Hubbard model of spinless fermions at half-filling. We investigate the model within two distinct Green's function approaches: In the first approach a single-site representation decoupling scheme is used that includes the effect of nearest neighbor charge fluctuations. In the second approach a cluster representation leading to a 'multiorbital' model is investigated which includes intra-cluster correlations more rigorously and those between clusters on a mean field basis. It is demonstrated that with increasing nearest-neighbor Coulomb interaction V both approaches lead to a metal-insulator transition with an associated 'Mott-Hubbard' like gap caused by V. Within the single site approach we also explore the possibility of charge order. Furthermore we investigate the evolution of the quasiparticle bands as funtion of V.

PACS. 71.30.+h Metal-insulator transitions and other electronic transitions – 71.10.Fd Lattice fermion models (Hubbard model, etc.) – 71.10.Pm Fermions in reduced dimensions (anyons, composite fermions, Luttinger liquid, etc.) – 71.27.+a Strongly correlated electron systems; heavy fermions

1 Introduction

To treat the problem of a metal-insulator transition (MIT) driven by electron-electron interactions in lattice models with a fractional electron site occupancy, both the on-site and long-range Coulomb repulsions are equally important [1]. A lattice with geometrical frustration imposes additional complications and may produce new features of MIT. The well known example is the Verwey transition [3] in magnetite (Fe_3O_4) at $T_V \approx 120$ K. Magnetite has a spinel structure and A sites are occupied regularly with Fe^{3+} ions. On the B sites forming a pyrochlore lattice, the Fe ions are in the mixed valent state of Fe^{2+}:Fe^{3+} = 1:1. Therefore, in the high-temperature charge disordered state, $T > T_V$, a band structure calculation would predict a quarter-filled conduction band, i.e., a metallic state with one itinerant electron per two sites. Below the Curie temperature $T_C \approx 850$ K of magnetite the itinerant electrons are (almost) fully ferromagnetically polarized. Therefore they can be treated as a system of interacting spinless fermions. In terms of spinless fermions, the charge occupancy of one electron per two sites corresponds to a half band-filling. Below the Verwey temperature T_V, the charge degrees of freedom are ordered and an insulating state occurs. As was first pointed out by Anderson [4], properties of the Verwey transition can not be understood without taking into account the geometrical frustration and the resulting huge degeneracy of the ground-state charge configurations in the pyrochlore lattice. Two more recent examples of electronic structure changes connected to charge ordering in spinels are found in AlV_2O_4 with temperature decreasing at ambient pressure [5,6] and in LiV_2O_4 under the external pressure [7,6]. An interesting observation is that charge ordering in these three spinel systems is accompanied with a lattice structural change, i.e., the system tries to avoid the geometrical frustration of the pyrochlore structure. At the same time, no MIT and charge ordering were observed in LiV_2O_4 at ambient pressure down to very low temperatures, but instead the metallic compound LiV_2O_4 exhibits a heavy-fermion behavior below 30 K [8,9].

Most of the work until now has been devoted to an understanding of the magnetic properties of geometrically frustrated lattices such as pyrochlore structure, since in the presence of antiferromagnetic interaction frustration acts against a conventional long-range order and may stabilize a spin-liquid state [10]. Charge degrees of freedom have in contrast been studied much less [11]. In fact,

[a] e-mail: yzhang@issp.u-tokyo.ac.jp; yzzhang@mpipks-dresden.mpg.de

charge ordering in geometrically frustrated systems has been an intriguing and unsettled problems [12]. For example, numerical diagonalizations of a Hamiltonian for spinless fermion with strong nearest-neighbor repulsion on a checkerboard lattice have given evidence that at half filling (number of spinless fermion equals one half the number of sites) the ground state is two-fold degenerate but a liquid [13]. This must be kept in mind when that system is treated within different approximations leading to a charge ordered ground state. In other words, the observed charge order in frustrated structures could crucially depend on associated lattice deformations, i.e., the involvement of lattice degree of freedom.

The extended Hubbard model on non-frustrated lattices has been extensively investigated in one dimension at quarter-[14] or half-filling [15], for two-leg ladders at quarter-filling [16], for two-dimensional square lattices at half-filling [17] and in the limit of infinite dimensions at quarter-[18] or half-filling [19]. A variety of techniques, such as Hartree-Fock approximation, pertubation theory, dynamical mean-field theory, as well as numerical methods, e.g., quantum Monte Carlo and density-matrix renormalization group have been employed. However all these investigations were based on the non-frustrated lattice.

In the present paper, we apply a Green's function approach to study the possible phase transitions of a half-filled spinless fermion model, i.e., a system with one electron per two sites, on the frustrated checkerboard lattice (see the inset of Fig. 1). The lattice can be viewed as a two-dimensional projection of a pyrochlore lattice. The spinless fermion model arises naturally for ferromagnetic materials in which one of the spin-split bands is completely occupied or completely empty as in magnetite [20]. Also this model can be viewed as a quarter-filled extended Hubbard model in the large U limit. Then double occupancy of a site is forbidden and the nearest-neighbour Coulomb repulsion V plays a crucial role. Because for (spinless) half filling every second site is unoccupied on the average one would naively expect a metallic state. Our main goal in this work is to show that inter-site correlations V can lead to a MI transition even for a case with less than one electron per site. We are using two different methods to study this model.

Firstly we employ a single site approach within a Hartree-Fock as well as Hubbard-I type approximations (Sect. 2). By using the 'Hubbbard-I'-type decoupling scheme which includes the effect of nearest-neighbor charge fluctuations, we find that with increasing value of V first a metal-insulator transition occurs with a gap in the excitation spectrum, while at even larger values of V charge ordering appears. This is opposite to the result in the simple Hartree-Fock approximation, i.e. inter-site correlations favor the MI transition and suppress the CO. This observation may indicate that CO is indeed not present for a rigid checkerboard or pyrochlore lattice for any V/t ratio (it certainly is not in the limit $V/t \to \infty$). Indeed in the compounds AlV_2O_4 and LiV_2O_4 (under pressure) where CO has been found it is accompanied by a lattice distortion.

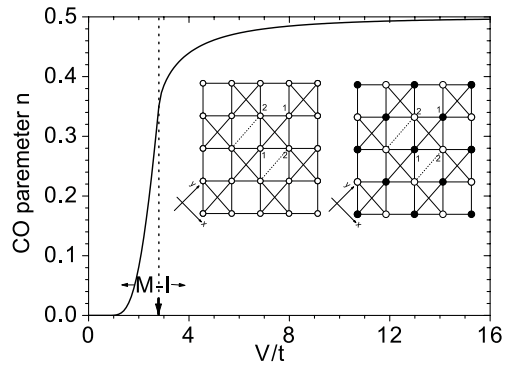

Fig. 1. Charge order parameter n as a function of V/t within a mean-field approximation. Dotted line indicates the critical point of the metal-insulator transition. Inset is an illustration of the checkerboard lattice with (right) and without (left) charge order. The **l**-th unit cell is indicated by dotted lines. The wave vector of the staggered CO is $\mathbf{Q} = (0, 0)$ due to the two sites per unit cell. Here charge order occurs before the metal-insulator transition takes place.

Secondly we start from a cluster representation of the model where the intra-cluster Coulomb interaction is taken into account exactly and the inter-cluster Coulomb term is treated in Hartree Fock approximation (Sect. 3). This transformation leads to an effective multi-orbital extended Hubbard model. Again we find a M-I transition at a value similar to the first approach. In view of the suggestion above we do not consider the possibility of CO in this case, although within the Hartree Fock approximation for the inter-cluster interactions it would presumably be present in the ground state.

Furthermore, we investigated the evolution of quasiparticle bands in the various phases in the single-site and cluster approaches. Following the selfconsistently determined chemical potential and the formation of interband gaps allows to determine the critical value for the MI transition.

2 Single site approximation

The Hamiltonian for the spinless fermion model is given by [11]

$$H = -t \sum_{\langle ij \rangle} c_i^\dagger c_j + V/2 \sum_{\langle ij \rangle} n_i n_j \tag{1}$$

where V is the Coulomb repulsion between nearest neighbors denoted by $\langle ij \rangle$. We refer to this spinless Hamiltonian as the $t - V$ model.

First, let us briefly review previous work on the $t - V$ model at half-filling and the closely related quarter-filled extended Hubbard model in the large U limit for different lattices. In one dimension, the $t - V$ model can be mapped onto an anisotropic Heisenberg model [21] and solved exactly via Bethe ansatz. In this case, one finds a gapless metallic phase for $V < 2t$ and a gapped charge-ordered state for larger values of V. For $t - V$ model on a two-leg ladder, it was found from renomalization group

calculations that contrary to a single chain, the ladder becomes a Mott insulator for arbitrarily small repulsive interactions V [22]. By using the density matrix renormalization group method, Vojta [16] et al. studied the extended Hubbard model for two-leg ladders in the large U limit. They found that the charge-ordered phase vanishes for $V < 2.5t$ but claimed that there will be a charge gap for all values of V/t. For a square lattice, McKenzie [23] et al. argued from slave-boson theory that the insulating phase with charge order is destroyed below a critical value V of order t and the system becomes metallic.

Here we will study the $t-V$ model on the checkerboard lattice at half-filling (one electron per two sites) with the aim to find out about possible MI and CO transitions in this frustrated lattice which is a 2D model for the pyrochlore lattice. At first we will employ the Green's function method and various decoupling schemes within the single-site representation. There are two sites per unit cell. For convenience, we rewrite the Hamiltonian (1) in the following form

$$H = H_t + H_{V,MF} + H'_V, \tag{2}$$

where

$$H_t = -t\sum_{\mathbf{l}}\Big[c^\dagger_{\mathbf{l},2}\left(c_{\mathbf{l}-\mathbf{x}-\mathbf{y},1} + c_{\mathbf{l}-\mathbf{y},1} + c_{\mathbf{l}+\mathbf{x},2}\right) + c^\dagger_{\mathbf{l},1}\left(c_{\mathbf{l},2} + c_{\mathbf{l}+\mathbf{x},2} + c_{\mathbf{l}-\mathbf{y},1}\right) + \text{h.c.}\Big], \tag{3}$$

$$\begin{aligned} H_{V,MF} = V\sum_{\mathbf{l}}\big[&n_{\mathbf{l},2}\left(\langle n_{\mathbf{l}-\mathbf{x}-\mathbf{y},1} + n_{\mathbf{l}-\mathbf{y},1} + n_{\mathbf{l}+\mathbf{x},2}\rangle\right) \\ &+ \langle n_{\mathbf{l},2}\rangle\left(n_{\mathbf{l}-\mathbf{x}-\mathbf{y},1} + n_{\mathbf{l}-\mathbf{y},1} + n_{\mathbf{l}+\mathbf{x},2}\right) \\ &+ n_{\mathbf{l},1}\left(\langle n_{\mathbf{l},2} + n_{\mathbf{l}+\mathbf{x},2} + n_{\mathbf{l}-\mathbf{y},1}\rangle\right) \\ &+ \langle n_{\mathbf{l},1}\rangle\left(n_{\mathbf{l},2} + n_{\mathbf{l}+\mathbf{x},2} + n_{\mathbf{l}-\mathbf{y},1}\right) \\ &- \langle n_{\mathbf{l},2}\rangle\left(\langle n_{\mathbf{l}-\mathbf{x}-\mathbf{y},1} + n_{\mathbf{l}-\mathbf{y},1} + n_{\mathbf{l}+\mathbf{x},2}\rangle\right) \\ &- \langle n_{\mathbf{l},1}\rangle\left(\langle n_{\mathbf{l},2} + n_{\mathbf{l}+\mathbf{x},2} + n_{\mathbf{l}-\mathbf{y},1}\rangle\right)\big], \end{aligned} \tag{4}$$

$$\begin{aligned} H'_V = V\sum_{\mathbf{l}}\big[&\delta n_{\mathbf{l},2}\left(\delta n_{\mathbf{l}-\mathbf{x}-\mathbf{y},1} + \delta n_{\mathbf{l}-\mathbf{y},1} + \delta n_{\mathbf{l}+\mathbf{x},2}\right) \\ &+\delta n_{\mathbf{l},1}\left(\delta n_{\mathbf{l},2} + \delta n_{\mathbf{l}+\mathbf{x},2} + \delta n_{\mathbf{l}-\mathbf{y},1}\right)\big]. \end{aligned} \tag{5}$$

Here we have introduced a charge fluctuation operator $\delta n_{\mathbf{l},i} = n_{\mathbf{l},i} - \langle n_{\mathbf{l},i}\rangle$ on sites $i = 1, 2$ of the $\mathbf{l}$-th cell. H_t is the kinetic energy term, $H_{V,MF}$ is mean-field part of the interaction term while H'_V is the residual interaction part. In the following we only consider the simplest charge ordered pattern, namely a staggered checkerboard pattern with wave vector $\mathbf{Q} = (0, 0)$ illustrated in the inset of Figure 1. The average charge density on different sites in the cell is $\langle n_{\mathbf{l},i}\rangle = \frac{1}{2} - (-1)^i n$, where the order parameter n means a charge disproportionation within each unit cell. We now briefly discuss the motivation for considering this order parameter of the 2D checkerboard lattice. Firstly it corresponds precisely to the one considered as the proper candidate for the Verwey transition in the 3D pyrochlore or spinel- type lattices such as mangetite [3]. Secondly it is the only type of charge order with only two sublattices. For this case the quasiparticle poles of the Green's functions can be obtained explicitly, which is a precondition for the self consistent determination of the order parameter amplitude as a function of V/t.

The electron propagation is described by a retarded Green's function (for simplicity the conventional symbol R is omitted)

$$G_{ij}\left(\mathbf{l}-\mathbf{l}',\omega\right) = \left\langle\left\langle c_{\mathbf{l}i}|c^\dagger_{\mathbf{l}'j}\right\rangle\right\rangle_\omega = \int\left\langle\left\langle c_{\mathbf{l}i}(t)|c^\dagger_{\mathbf{l}'j}\right\rangle\right\rangle e^{i\omega t}dt. \tag{6}$$

where

$$\left\langle\left\langle c_{\mathbf{l}i}(t)|c^\dagger_{\mathbf{l}'j}\right\rangle\right\rangle = -i\theta\left(t\right)\left\langle\left\{c_{\mathbf{l}i}\left(t\right), c^\dagger_{\mathbf{l}'j}\left(0\right)\right\}\right\rangle. \tag{7}$$

and $\{,\}$ denotes the anticommutator. The above (2×2)-matrix Green's function must satisfy the equation

$$\omega\left\langle\langle A|B\rangle\right\rangle_\omega = \langle\ \{A, B\}\rangle + \left\langle\langle[A, H]\,|B\rangle\right\rangle_\omega. \tag{8}$$

By introducing the Fourier transformation

$$G_{ij}\left(\mathbf{k},\omega\right) = \frac{1}{N}\sum_{\mathbf{k}} e^{i\mathbf{k}\cdot\left(\mathbf{R}_{\mathbf{l}}-\mathbf{R}'_{\mathbf{l}}\right)}G_{ij}\left(\mathbf{l}-\mathbf{l}',\omega\right), \tag{9}$$

the equation (8) can be now written explicitly as

$$\left(\omega\widehat{1} + \widehat{\Lambda}\left(\mathbf{k}\right)\right)\widehat{G}\left(\mathbf{k},\omega\right) = \widehat{1} + V\widehat{\Gamma}\left(\mathbf{k},\omega\right). \tag{10}$$

with

$$\widehat{\Lambda}\left(\mathbf{k}\right) = \begin{pmatrix} -\left(3-2n\right)V + 2t\cos k_y & 4te^{-i\frac{k_x+k_y}{2}}\cos\frac{k_x}{2}\cos\frac{k_y}{2} \\ 4te^{i\frac{k_x+k_y}{2}}\cos\frac{k_x}{2}\cos\frac{k_y}{2} & -\left(3+2n\right)V + 2t\cos k_x \end{pmatrix}, \tag{11}$$

where $\widehat{1}$ is the unit matrix and $\widehat{\Gamma}\left(\mathbf{k},\omega\right)$ is the Fourier transformation of the (2×2) higher-order matrix Green's function which is defined as

$$\Gamma_{ij}\left(\mathbf{l}-\mathbf{l}',\omega\right) = \left\langle\left\langle c_{\mathbf{l},i}\sum_{(n.n.)\in(\mathbf{l},i)}\delta n_{(n.n.)}|c^\dagger_{\mathbf{l}',j}\right\rangle\right\rangle_\omega. \tag{12}$$

Here the summation is over six nearest-neighbor sites (n.n.) surrounding the site $(\mathbf{l}, i)$

2.1 Mean-field approximation

In the first step we may decouple

$$\Gamma_{ij}\left(\mathbf{l}-\mathbf{l}',\omega\right) \approx \left\langle\sum_{(n.n.)\in(\mathbf{l},i)}\delta n_{(n.n.)}\right\rangle\left\langle\left\langle c_{\mathbf{l},i}|c^\dagger_{\mathbf{l}',j}\right\rangle\right\rangle_\omega = 0, \tag{13}$$

which leads to a mean-field approximation and the quasiparticle dispersions are given by

$$\begin{aligned} E^\pm_{\mathbf{k}}/t = &-(\cos k_x + \cos k_y - 3V/t) \\ &\pm\left[4(1+\cos k_x)(1+\cos k_y)\right. \\ &\left.+ (2nV/t - \cos k_x + \cos k_y)^2\right]^{1/2}. \end{aligned} \tag{14}$$

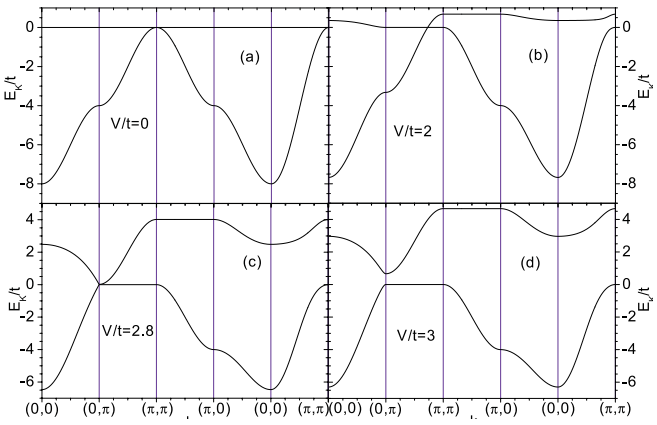

Fig. 2. Quasiparticle dispersion within mean-field theory for different value of V/t. The chemical potential μ is fixed at zero energy. (a) is the noninteracting case without charge order. These two bands touch at (π,π) and the upper band is flat. (b) is in the metallic phase with small charge order. The two bands still touch while the upper band become dispersive due to the inequivalence of diagonal hopping. (c) is exactly at the critical point. The two bands touch at $(0,\pi)$. (d) is in the insulating phase. The two bands seperate.

Now the intra-cell charge disproportionation n has to be determined from the following self-consistent equation

$$n = \frac{1}{2N}\sum_{\underline{k}} \frac{(2nV/t - \cos k_x + \cos k_y)}{\left[4(1+\cos k_x)(1+\cos k_y) + (2nV/t - \cos k_x + \cos k_y)^2\right]^{1/2}}. \quad (15)$$

The calculated phase diagram is shown in Figure 1. In the present mean-field approximation ($\widehat{\Gamma} \equiv 0$) the metallic phase is already charge ordered before a charge-transfer-type metal-insulator phase transition takes place at $V = 2.8t$. In the non-interacting case $V = 0$ (Fig. 2a), the upper band is flat while the lower band is dispersive. It touches the flat band at (π,π). As shown in Figures 2b, 2c with increasing intersite repulsion V the flat band becomes increasingly dispersive with increasing charge order and the touching point moves from (π,π) towards $(0,\pi)$. The dispersion of the previously flat band is due to the inequivalence of diagonal hopping (see inset of Fig. 1) induced by charge order. Finally, for $V > 2.8t$ the two bands separate as shown in Figure 2d. In the half-filled case, the lower band is fully occupied and the upper band is empty resulting in a charge-transfer-type insulator.

2.2 'Hubbard I'- approximation for the inter-site correlations

The neglect of correlations overestimates the tendency to CO symmetry breaking. Therefore, in the strongly correlated case ($V \gg t$), the mean-field results are unreliable and it is necessary to consider equations of motion of higher-order Green's functions $\Gamma_{ij}(\mathbf{l}-\mathbf{l}',\omega)$ which can be written as

$$\begin{aligned}
&\left(\omega - V\sum_{(n.n.)\in(\mathbf{l},i)}\langle n_{(n.n.)}\rangle\right)\\
&\times\left\langle\left\langle c_{\mathbf{l},i}\sum_{(n.n.)\in(\mathbf{l},i)}\delta n_{(n.n.)}|c^{\dagger}_{\mathbf{l}',j}\right\rangle\right\rangle_{\omega} =\\
&\sum_{(n.n.)\in(\mathbf{l},i)}\delta_{(\mathbf{l}',j),(n.n.)}\left\langle c_{\mathbf{l}i}c^{\dagger}_{(n.n.)}\right\rangle\\
&-t\sum_{(n.n.)\in(\mathbf{l},i)}\left\langle\left\langle c_{(n.n.)}\delta n_{\mathbf{l},i}|c^{\dagger}_{\mathbf{l}',j}\right\rangle\right\rangle_{\omega}\\
&-t\sum_{(n.n.)\in(\mathbf{l},i)}\left(\langle n_{\mathbf{l},i}\rangle - \langle n_{n.n.}\rangle\right)\left\langle\left\langle c_{(n.n.)}|c^{\dagger}_{\mathbf{l}',j}\right\rangle\right\rangle_{\omega}\\
&-t\sum_{(n.n.)\in(\mathbf{l},i)}\sum_{(n.n.)'\in(\mathbf{l},i)}\left(1-\delta_{(n.n.)',(n.n.)}\right)\\
&\times\left\langle\left\langle c_{(n.n.)'}\delta n_{(n.n.)}|c^{\dagger}_{\mathbf{l}',j}\right\rangle\right\rangle_{\omega}\\
&-t\sum_{(n.n.)\in(\mathbf{l},i)}\sum_{(n.n.)'\in(n.n.)}\left(1-\delta_{(n.n.)',(\mathbf{l},i)}\right)\\
&\times\left\langle\left\langle c_{\mathbf{l},i}c^{+}_{(n.n.)}c_{(n.n.)'}|c^{\dagger}_{\mathbf{l}',j}\right\rangle\right\rangle_{\omega}\\
&+t\sum_{(n.n.)\in(\mathbf{l},i)}\sum_{(n.n.)'\in(n.n.)}\left(1-\delta_{(n.n.)',(\mathbf{l},i)}\right)\\
&\times\left\langle\left\langle c_{\mathbf{l},i}c^{+}_{(n.n.)'}c_{(n.n.)}|c^{\dagger}_{\mathbf{l}',j}\right\rangle\right\rangle_{\omega}\\
&+V\left\langle\left\langle c_{\mathbf{l},i}\left(\sum_{(n.n.)\in(\mathbf{l},i)}\delta n_{(n.n.)}\right)^2|c^{\dagger}_{\mathbf{l}',j}\right\rangle\right\rangle_{\omega}. \quad (16)
\end{aligned}$$

Here we adopt the following approximations, which consist in an extension of the on-site Hubbard I decoupling scheme [24] to spinless fermion on a checkerboard lattice with intersite Coulomb interaction:

$$\begin{aligned}
&\left\langle\left\langle c_{\mathbf{l},i}\left(c^{+}_{(n.n.)}c_{(n.n.)'} - c^{+}_{(n.n.)'}c_{(n.n.)}\right)|c^{\dagger}_{\mathbf{l}',j}\right\rangle\right\rangle_{\omega} \simeq\\
&\left(\left\langle c^{+}_{(n.n.)}c_{(n.n.)'}\right\rangle - \left\langle c^{+}_{(n.n.)'}c_{(n.n.)}\right\rangle\right)\left\langle\left\langle c_{\mathbf{l},i}|c^{\dagger}_{\mathbf{l}',j}\right\rangle\right\rangle_{\omega}\\
&= 0. \quad (17)
\end{aligned}$$

In equation (16), the fourth term involves both the nearest- and next-nearest-neighbor charge correlations and we neglect the latter. When treating the last term in equation (16) we also neglect the more distant charge

correlations and approximate as

$$\left\langle\left\langle c_{\mathbf{l},1}\left(\sum_{(n.n.)\in(\mathbf{l},1)}\delta n_{(n.n.)}\right)^2|c^{\dagger}_{\mathbf{l}',j}\right\rangle\right\rangle_{\omega}\simeq$$
$$\left\langle\left(\sum_{(n.n.)\in(\mathbf{l},1)}\delta n_{(n.n.)}\right)^2\right\rangle\left\langle\left\langle c_{\mathbf{l},1}|c^{\dagger}_{\mathbf{l}',j}\right\rangle\right\rangle_{\omega}\simeq$$
$$\left(\frac{3}{2}-6n^2+2\left\langle\delta n_{\mathbf{l},2}\sum_{(n.n.)\in(\mathbf{l},2)}\delta n_{(n.n.)}\right\rangle\right)$$
$$\times\left\langle\left\langle c_{\mathbf{l},1}|c^{\dagger}_{\mathbf{l}',j}\right\rangle\right\rangle_{\omega}. \quad (18)$$

Finally the equation of motion for the higher-order Green's function $\Gamma_{ij}(\mathbf{k},\omega)$ can be written as

$$\left(\omega\widehat{1}+\widehat{\Lambda}(\mathbf{k})\right)\widehat{\Gamma}(\mathbf{k},\omega)=\widehat{B}(\mathbf{k})+\widehat{M}(\mathbf{k})\widehat{G}(\mathbf{k},\omega). \quad (19)$$

where

$$\widehat{M}(\mathbf{k})=\begin{pmatrix} VK_2 & -8nte^{-i\frac{k_x+k_y}{2}}\times\cos\frac{k_x}{2}\cos\frac{k_y}{2} \\ 8nte^{i\frac{k_x+k_y}{2}}\times\cos\frac{k_x}{2}\cos\frac{k_y}{2} & VK_1\end{pmatrix}, \quad (20)$$

and

$$\widehat{B}(\mathbf{k})=\begin{pmatrix} 2\left\langle c_{\mathbf{l}1}c^{\dagger}_{\mathbf{l}-\mathbf{y}1}\right\rangle\cos k_y & 4\left\langle c_{\mathbf{l}1}c^{\dagger}_{\mathbf{l}2}\right\rangle e^{-i\frac{k_x+k_y}{2}}\times\cos\frac{k_x}{2}\cos\frac{k_y}{2} \\ 4\left\langle c_{\mathbf{l}1}c^{\dagger}_{\mathbf{l}2}\right\rangle e^{i\frac{k_x+k_y}{2}}\times\cos\frac{k_x}{2}\cos\frac{k_y}{2} & 2\left\langle c_{\mathbf{l}2}c^{\dagger}_{\mathbf{l}+\mathbf{x}2}\right\rangle\cos k_x\end{pmatrix}. \quad (21)$$

Here we used the definition

$$K_i=\left(\frac{3}{2}-6n^2+2\left\langle\delta n_{\mathbf{l},i}\sum_{(n.n.)\in(\mathbf{l},i)}\delta n_{(n.n.)}\right\rangle\right). \quad (22)$$

By solving equation (19) with respect to $\widehat{\Gamma}$ and after substituting $\widehat{\Gamma}$ into equation (10) one obtains the final solution for the Green's function $\widehat{G}$. For the electron concentration 1/2 (one electron per unit cell), the chemical potential μ, the charge disproportionation n and the hopping amplitude $\left\langle c_{\mathbf{l}1}c^{\dagger}_{\mathbf{l}2}\right\rangle$ are calculated from the following set of self-consistent equations:

$$1=\frac{1}{N/2}\sum_{\mathbf{k}}\int_{-\infty}^{\mu}d\omega\left(-\frac{1}{\pi}\right)\mathrm{Im}\left[G_{11}(\mathbf{k},\omega)+G_{22}(\mathbf{k},\omega)\right], \quad (23)$$

$$n=\frac{1}{N/2}\sum_{\mathbf{k}}\int_{-\infty}^{\mu}d\omega\left(-\frac{1}{\pi}\right)\mathrm{Im}\left[\frac{G_{11}(\mathbf{k},\omega)-G_{22}(\mathbf{k},\omega)}{2}\right], \quad (24)$$

$$\left\langle c_{\mathbf{l}1}c^{\dagger}_{\mathbf{l}2}\right\rangle=\frac{1}{N/2}\sum_{\mathbf{k}}\int_{-\infty}^{\mu}d\omega\left(-\frac{1}{\pi}\right)\mathrm{Im}\,G_{12}(\mathbf{k},\omega). \quad (25)$$

The higher-order Green's function $\Gamma_{ij}(\mathbf{k},\omega)$ can be easily derived from equation (10). Therefore the nearest-neighbor charge fluctuation correlation $\left\langle\delta n_{\mathbf{l},i}\sum_{(n.n.)\in(\mathbf{l},i)}\delta n_{(n.n.)}\right\rangle$ can be calculated as

$$\left\langle\delta n_{\mathbf{l}i}\sum_{(n.n.)\in(\mathbf{l},i)}\delta n_{(n.n.)}\right\rangle=\frac{1}{N/2}\sum_{\mathbf{k}}\int_{-\infty}^{\mu}d\omega\left(-\frac{1}{\pi}\right)\mathrm{Im}\,\Gamma_{ii}(\mathbf{k},\omega). \quad (26)$$

Furthermore the hopping amplitude $\left\langle c_{\mathbf{l}1}c^{\dagger}_{\mathbf{l}-\mathbf{y}1}\right\rangle$ and $\left\langle c_{\mathbf{l}2}c^{\dagger}_{\mathbf{l}+\mathbf{x}2}\right\rangle$ can be also determined from $G_{11}(\mathbf{k},\omega)$ and $G_{22}(\mathbf{k},\omega)$ respectively.

The one-particle retarded Green's function exhibits four poles given by the roots of $D=0$ where D is defined as

$$\begin{aligned}D=&\left(\omega-E^{+}_{\mathbf{k}}\right)^2\left(\omega-E^{-}_{\mathbf{k}}\right)^2+V^4K_1K_2\\&+16n^2V^2t^2(1+\cos k_x)(1+\cos k_y)\\&-V^2K_1[(\omega-(3-2n)V+2t\cos k_y)^2\\&-4t^2(1+\cos k_x)(1+\cos k_y)]\\&-V^2K_2[(\omega-(3+2n)V+2t\cos k_x)^2\\&-4t^2(1+\cos k_x)(1+\cos k_y)].\end{aligned} \quad (27)$$

As a consequence, four bands are obtained. For $V=0$, two branches of momentum-dependent dispersions are obtained from equation (27): $E^{-}_{\mathbf{k}}|_{V=0}=-2t(\cos k_x+\cos k_y+1)$ and $E^{+}_{\mathbf{k}}|_{V=0}=2t$ as expected. When $t=0$, two poles $\omega=2V$ and $\omega=4V$ are obtained from above equations, which describes one hole or one particle excitation.

In Figure 3a we show the phase diagram within the previously used decoupling scheme. First, a metal-insulator transition occurs at $V_{c1}=4.86t$ and then charge ordering appears at $V_{c2}=6.47t$. In the interval $V>V_{c1}$ and $V<V_{c2}$ a gap opens and increases with increasing value of V. At V_{c2}, it drops to a smaller value. For $V>V_{c2}$,

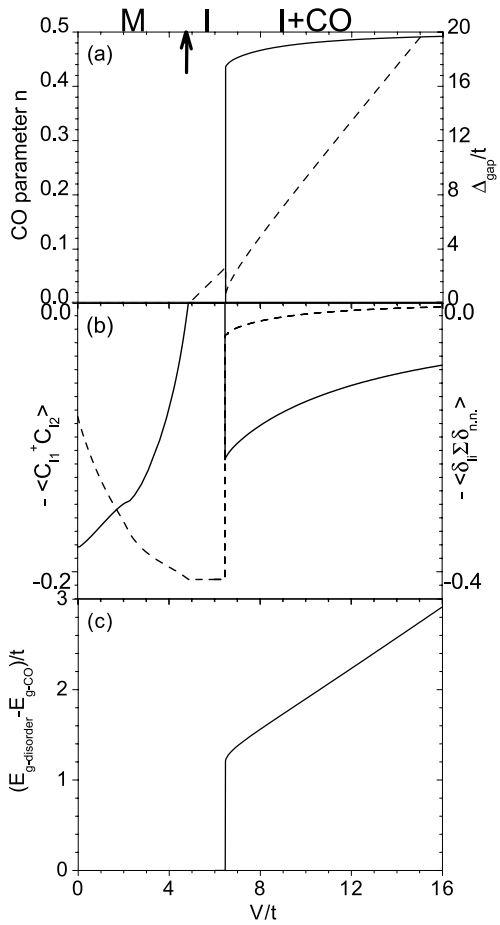

Fig. 3. Results within Hubbard I-like approximation. Full(dashed) lines correspond to left (right) ordinates and labels. (a) charge order (CO) parameter n versus V/t (left label). The arrow indicates the phase boundary between the metallic and insulating phase without charge ordering. In contrast to the mean-field approximation, the charge-ordered phase transition is of first order and occurs *a*fter a Mott-Hubbard-like metal-insulator transition has taken place. The dashed line shows the quasiparticle gap versus V/t in both insulating phases (right label). (b) Hopping amplitude (solid line) from site 2 to site 1 ($\left\langle c_{\mathbf{l}1}^{\dagger}c_{\mathbf{l}2}\right\rangle$) (left label) and nearest-neighbor charge fluctuation correlations $\left\langle \delta n_{\mathbf{l}i}\sum_{(n.n.)\in(\mathbf{l},i)}\delta n_{(n.n.)}\right\rangle$ (dashed line, right label) versus V/t. (c) Energy difference between ordered and disordered state versus V/t. For $V > V_{c2}$, the charge-ordered state has lower energy.

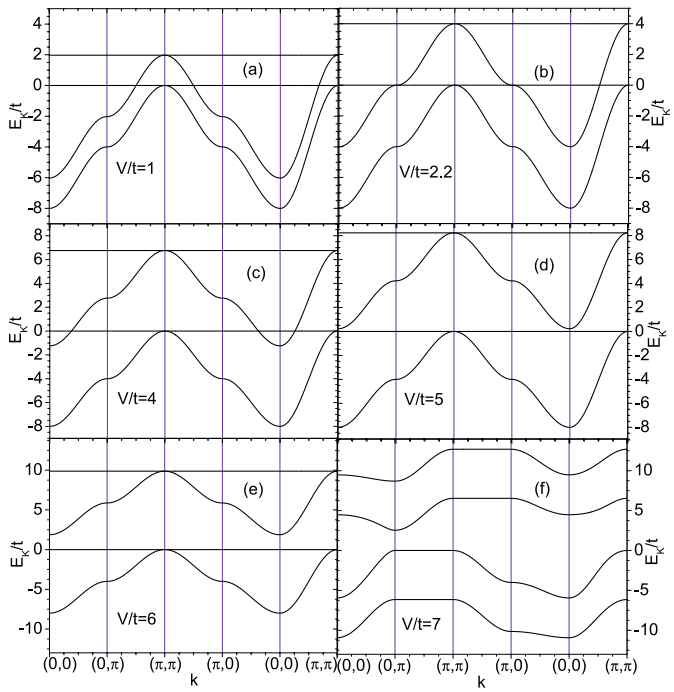

Fig. 4. evolution of the quasiparticle spectrum within a Hubbard I-like approximation for different value of V/t. The chemical potential μ is fixed at zero energy. $V/t = 0$ is already shown in Figure 2a. Figures (a), (b) and (c) are in the metallic phase ($0 < V < V_{c1} = 4.86t$). Figures (d) and (e) are in the insulating phase without CO symmetry breaking ($V_{c1} < V < V_{c2} = 6.47t$). Reminiscent of the upper and lower Hubbard band splitting, the metal-insulator phase transition at V_{c1} is of Mott-Hubbard type. Figure (f) is in the insulating phase with CO ($V > V_{c2}$).

the gap increases again monotonously. In the charge ordered phase, there exist always two self-consistent solutions, i.e., a charge ordered and a disordered one. By comparing the energy of these two states, (see Fig. 3c), we find for $V > V_{c2}$ that the charge ordered state has lower energy. The phase transition is of first order. Figure 3b shows that at the metal-insulator transition the hopping amplitude $\left\langle c_{\mathbf{l}1}c_{\mathbf{l}2}^{\dagger}\right\rangle$ vanishes.

In the following we want to explain this feature in more detail. For that purpose we study the poles of the retarded Green's function as a function of increasing value of V/t. Consider first the trivial case of $V = 0$ (see Fig. 2a). The states in the dispersive band are of bonding and in the flat band of antibonding character. As seen in Figures 4a, b and c these bands split into four when $0 < V < V_{c1}$ and the Hubbard-I like approximation is made. The retarded Green's function has therefore four poles for each $\mathbf{k}$ vector. In the regime $0 < V < V_{c1}$, states in the antibonding flat band become more and more occupied as V increases. Therefore the expectation value $\left\langle c_{\mathbf{l}1}^{\dagger}c_{\mathbf{l}2}\right\rangle$ decreases since an equal occupational probability of a bonding and antibonding state implies that $\left\langle c_{\mathbf{l}1}^{\dagger}c_{\mathbf{l}2}\right\rangle = 0$. This is the case in the regime $V_{c1} < V < V_{c2}$ shown in Figures 4d, e. Note that a correlation gap has opened above the two occupied lower bands which implies a Mott-Hubbard type insulating state and the nearest-neighbor charge fluctuation correlations $\delta n_{\mathbf{l}i}\sum_{(n.n.)\in(\mathbf{l},i)}\delta n_{(n.n.)}$ remain constant. When $V > V_{c2}$, then due to symmetry breaking one can no longer distinguish between bonding and antibonding state and $\left\langle c_{\mathbf{l}1}^{\dagger}c_{\mathbf{l}2}\right\rangle \neq 0$ (see Figs. 4f). As V continues to increase, charge order become more and more pronounced and $\left\langle c_{\mathbf{l}1}^{\dagger}c_{\mathbf{l}2}\right\rangle$ decreases again monotonously. This explains

the behavior of $\left\langle c_{\mathbf{l}1}^{\dagger} c_{\mathbf{l}2} \right\rangle$ shown in Figure 3. The inflexion point at $V/t = 2.2$ shown in Figure 3b is due to the lower flat band crossing the inflexion points (maximum of DOS) of the upper dispersive band shown in Figure 4b. For $V > V_{c2}$, CO strongly suppresses the nearest-neighbor charge fluctuation correlations $\delta n_{\mathbf{l}i} \sum_{(n.n.)\in(\mathbf{l},i)} \delta n_{(n.n.)}$ which is site-independent for all value of V/t as expected.

In this section we have studied the half-filled (one electron per two sites) spinless $t-V$ model on a checkerboard lattice within mean field theory and a 'Hubbard-I type' approach. In the former approximation which overestimates the tendency to symmetry breaking, CO appears before the system becomes an insulator. By using a Green's function approach and a decoupling scheme that includes the effect of nearest-neighbor charge fluctuations, however, it was shown that *first* a MI transition into an insulating state without CO takes place and only for larger V eventually CO appears. It is presently not clear, however, whether the ground state really exhibits charge order for finite V/t. It is known that in the limit ($V/t \to \infty$) when the hopping vanishes, the ground state for half filled checkerboard lattice has a macroscopic degeneracy [11,25] given by $(4/3)^{\frac{3N}{4}}$ which increases exponentially with the number of lattice sites N. This highly degenerate state has strong local charge correlations described by the tetrahedron rule [4] but it has no long range charge ordering [26]. It is therefore possible that CO obtained here for the rigid checkerboard lattice above V_{c2} and for finite t may be due to the employed approximation. In fact, the Verwey-type charge ordered state obtained here is one of the macroscopically degenerate states that obeys the tetrahedron rule. If there occurs a corresponding lattice distortion, for example, a compression along the diagonal direction [12], the system would select such a CO state shown in the inset of Figure 1 out of the macroscopically degenerate states. Indeed in some 3D pyrochlore compounds which exhibit CO as mentioned in the introduction, it is always accompanied by symmetry lowering lattice distortions which remove the frustration by introducing inequivalent bond lengths in the tetrahedrons of the corner sharing lattice. Theoretically this has been described by adding a deformation potential coupling of spinless fermions to the lattice and the elastic energy of associated symmetry strains in the Hamiltonian (1). It has been shown within unrestricted Hartree Fock approximation that this leads to a first order transition into a charge ordered state with spontaneous lattice distortion [6]. It seems possible that the extended CO model with lattice coupling can also be treated within the present HubbardI-type approximation.

As compared to the previous mean field approximation we found that the Hubbard I decoupling scheme suppresses the tendency to charge order in favor of a M-I transition without symmetry breaking. At this point it is appropriate to compare to the CO on the simple 2D square lattice (without the crosses in the inset of Fig. 1.) In the simple square lattice there is no frustration present. Therefore even on the rigid square lattice a transition to an only doubly degenerate charge ordered state of the type illustrated in Figure 1 (without the crosses) will occur for $V > V_c = 0.93t$. Because only a single n.n. tight binding band is present now the CO will remove the Fermi surface (for spinless half filling) and the CO transition will coincide with a transition to a charge transfer insulator, contrary to the case of the checkerboard lattice discussed here.

3 Cluster approximation

We want to supplement the previous calculation based on a Hubbard I type of approximation by another one where the strong electron correlations are treated more rigorously within a cluster but within mean-field approximation outside the cluster. Within this scheme we want to determine the critical interaction V_{c1} at which a gap opens in the excitation spectrum when the case of half-filling is considered. We do not care here about a possible charge order at large value of V because, as pointed out before, that may turn out to be an artefact of the involved approximations.

We divide the checkerboard lattice into sublattice A and B of the plaquette so that each sublattice contains $N/4$ units where N is the number of sites. Figure 5 shows black (basic) clusters linked across white square. The Hamiltonian (1), $H = H_t + H_V$, is decomposed into

$$H_t = H_t^{(intra)} + H_t^{(inter)}; \quad H_V = H_V^{(intra)} + H_V^{(inter)}. \quad (28)$$

Here each of the terms, $H_t^{(intra)}$ and $H_V^{(intra)}$, is a sum over $l = 1, ..., N/4$ decoupled basic clusters while $H_t^{(inter)}$ and $H_V^{(inter)}$are due to the intercluster coupling. Specifically the decoupled clusters are treated by the Hamiltonian

$$H_t^{(intra)} + H_V^{(intra)} = \sum_{\mathbf{l}} H_{t-V}^{(intra)}(\mathbf{l}) \quad (29)$$

$$H_{t-V}^{(intra)}(\mathbf{l}) = \sum_{i,j} M_{ij}(0) \left(-t c_{i\mathbf{l}}^{\dagger} c_{j\mathbf{l}} + \frac{V}{2} n_{i\mathbf{l}} n_{j\mathbf{l}} \right). \quad (30)$$

Here $i, j = 1, ..., 4$ denote the sites within a cluster with lattice vector $\mathbf{l}$ and $M_{ij}(0)$ is a (4×4)-matrix with elements $M_{ij}(0) = 1$, if $i \neq j$, and $M_{ii}(0) = 0$. Furthermore $n_{i\mathbf{l}} = c_{i\mathbf{l}}^{\dagger} c_{i\mathbf{l}}$. Thus, $H_{t-V}^{(intra)}(\mathbf{l})$ represents an intracluster Hamiltonian to be solved below.

To write down in a systematic way the intercluster coupling given by $H_t^{(inter)}$ and $H_V^{(inter)}$, we refer to Figure 5 where a fragment of the checkerboard lattice is shown with the origin located at the center of a basic cluster. There are eight neighboring basic clusters connected to a given one with the translation vectors $\{\boldsymbol{\tau}\} = \boldsymbol{\tau}_1, \boldsymbol{\tau}_2, ..., \boldsymbol{\tau}_8$. Three of them are depicted in Figure 5. The intercluster electron hopping and Coulomb repulsion terms can be written as

$$H_t^{(inter)} = -t \sum_{\mathbf{l}} \sum_{\{\boldsymbol{\tau}\}} \sum_{i,j} M_{ij}(\boldsymbol{\tau}) c_{i,\mathbf{l}+\boldsymbol{\tau}}^{\dagger} c_{j\mathbf{l}} \quad (31)$$

$$H_V^{(inter)} = \frac{V}{2} \sum_{\mathbf{l}} \sum_{\{\boldsymbol{\tau}\}} \sum_{i,j} M_{ij}(\boldsymbol{\tau}) n_{i,\mathbf{l}+\boldsymbol{\tau}} \, n_{j\mathbf{l}} \quad (32)$$

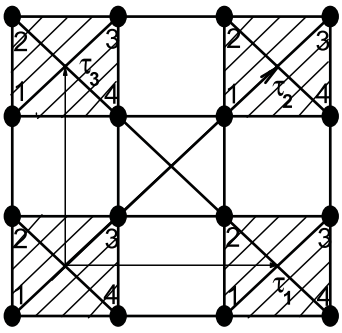

Fig. 5. Fragment of the checkerboard lattice. Only four neighboring basic clusters connected by elementary translation vectors τ_1, τ_2 and τ_3 are shown. Within each basic cluster the lattice sites are denoted by $1, ..., 4$.

where the eight (4×4)-matrices $M_{ij}(\boldsymbol{\tau})$ are specified by referring to Figure 5. Consider first the matrix $M_{ij}(\boldsymbol{\tau}_1)$ that connects two neighboring clusters by $\boldsymbol{\tau}_1$-translation. According to Figure 5, only two individual two-site bonds contribute to this connection (reading from the right to the left): $(ij) = (14), (23)$. Therefore, we define $M_{14}(\boldsymbol{\tau}_1) = M_{23}(\boldsymbol{\tau}_1) = 1$ and $M_{ij}(\boldsymbol{\tau}_1) = 0$ otherwise. In a similar way, one finds $M_{13}(\boldsymbol{\tau}_2) = 1, M_{12}(\boldsymbol{\tau}_3) = M_{43}(\boldsymbol{\tau}_3) = 1$ and $M_{ij}(\boldsymbol{\tau}_2) = M_{ij}(\boldsymbol{\tau}_3) = 0$ otherwise. With this procedure, the other five matrices $M_{ij}(\boldsymbol{\tau})$ can be easily found as well.

Now we solve the intra-cluster eigenvalue problem by diagonalizing the Hamiltonian $H_{t-V}^{(intra)}(\mathbf{l})$ from (30) separately in each n-particle $(n = 0, 1, ..., 4)$ sector

$$H_{t-V}^{(intra)}(\mathbf{l})\left|\Psi_\nu^{(n)}\right\rangle_{\mathbf{l}} = E_\nu^{(n)}\left|\Psi_\nu^{(n)}\right\rangle_{\mathbf{l}}. \tag{33}$$

The empty state $|\Psi_{\nu=1}^{(0)}\rangle_{\mathbf{l}}$ with energy $E_{\nu=1}^{(0)} = 0$ defines the cluster vacuum state $|0\rangle_{\mathbf{l}}$. There are four singly occupied cluster states $|\Psi_\nu^{(1)}\rangle_{\mathbf{l}}$ with $\nu = 1, ..., 4$ which are found to be

$$\left|\Psi_\nu^{(1)}\right\rangle_{\mathbf{l}} = \sum_{i=1}^{4} \beta_{\nu i} c_{i\mathbf{l}}^\dagger \left|0\right\rangle_{\mathbf{l}} \equiv f_{\nu\mathbf{l}}^\dagger \left|0\right\rangle_{\mathbf{l}} \tag{34}$$

where $\beta_{\nu i}$ is a (4×4)-matrix

$$\beta_{\nu i} = \frac{1}{2}\begin{pmatrix} 1 & 1 & 1 & 1 \\ 1 & -1 & 1 & -1 \\ \sqrt{2} & 0 & -\sqrt{2} & 0 \\ 0 & \sqrt{2} & 0 & -\sqrt{2} \end{pmatrix} \tag{35}$$

and the corresponding eigenvalues are

$$E_1^{(1)} = -3t; \quad E_2^{(1)} = E_3^{(1)} = E_4^{(1)} = t. \tag{36}$$

The eigenvectors (34) are basis vectors of different irreducible representations of C_{4h} point group: the case $\nu = 1$ describes the lowest energy fully symmetric (a_g) solution, $\nu = 2$ belongs to b_g and $\nu = 3, 4$ to e_u representation. Below we will refer to these 1-particle solutions as cluster 'orbitals'. According to (34), for a given cluster $\mathbf{l}$ the transformation from the original site operators $c_{i\mathbf{l}}^\dagger$ $(i = 1, ..., 4)$ to the cluster 'orbital' operators $f_{\nu\mathbf{l}}^\dagger$ is given by the matrix $\beta_{\nu i}$ defined in (35). Note that the $f_{\nu\mathbf{l}}^\dagger$ $(f_{\nu\mathbf{l}})$ operators anticommute. The cluster states of higher occupancy $n = 2, 3, 4$ can be understood as a result of successive filling of cluster 'orbitals'. For instance, for $n = 2$ one obtains six eigenstates (the cluster index $\mathbf{l}$ is dropped):

$$\left|\Psi_{1,2,3}^{(2)}\right\rangle = f_2^\dagger f_1^\dagger, f_3^\dagger f_1^\dagger, f_4^\dagger f_1^\dagger \left|0\right\rangle,$$
$$\left|\Psi_{4,5,6}^{(2)}\right\rangle = f_3^\dagger f_2^\dagger, f_4^\dagger f_2^\dagger, f_4^\dagger f_3^\dagger \left|0\right\rangle \tag{37}$$

with corresponding energies

$$E_{1,2,3}^{(2)} = -2t + V, \quad E_{4,5,6}^{(2)} = 2t + V. \tag{38}$$

In the cluster 'orbital' representation, the terms $H_t^{(intra)}$ and $H_V^{(intra)}$ in (29) can be now written as follows

$$H_t^{(intra)} = \sum_{\mathbf{l}} \left(-3t f_{1\mathbf{l}}^\dagger f_{1\mathbf{l}} + t \sum_{\nu=2}^{4} f_{\nu\mathbf{l}}^\dagger f_{\nu\mathbf{l}} \right), \tag{39}$$

$$H_V^{(intra)} = \frac{V}{2} \sum_{\mathbf{l}} \sum_{\nu=1}^{4} \sum_{\nu'(\neq\nu)} n_{\nu\mathbf{l}} n_{\nu'\mathbf{l}}. \tag{40}$$

From the result (40), one can see that $H_V^{(intra)}$ is the Hubbard term in an effective, 'multi-orbital' electronic model. Such a model is derived below by adding to (39) and (40) the intercluster hopping $H_t^{(inter)}$ and the Coulomb $H_V^{(inter)}$ terms and by using for the latter a mean-field approximation, i.e., $n_{i,\mathbf{l}+\boldsymbol{\tau}} n_{j\mathbf{l}} \simeq \langle n_{i,\mathbf{l}+\boldsymbol{\tau}} \rangle n_{j\mathbf{l}} + n_{i,\mathbf{l}+\boldsymbol{\tau}} \langle n_{j\mathbf{l}} \rangle - \langle n_{i,\mathbf{l}+\boldsymbol{\tau}} \rangle \langle n_{j\mathbf{l}} \rangle$. The approximated term $H_{V,MF}^{(inter)}$ reads

$$H_{V,MF}^{(inter)} = \frac{3}{4} \langle N_c \rangle V \sum_{\mathbf{l}} \sum_{i=1}^{4} n_{i\mathbf{l}} = \frac{3}{4} \langle N_c \rangle V \sum_{\mathbf{l}} \sum_{\nu=1}^{4} n_{\nu\mathbf{l}}, \tag{41}$$

where the last equality is due to $\sum_i n_{i\mathbf{l}} = \sum_\nu n_{\nu\mathbf{l}}$, and $\langle N_c \rangle = \sum_\nu \langle n_{\nu\mathbf{l}} \rangle$ is the average cluster occupancy. In the cluster 'orbital' representation, the hopping term $H_t^{(inter)}$ takes the following transparent form

$$H_t^{(inter)} = \sum_{\mathbf{l}} \sum_{\{\boldsymbol{\tau}\}} \sum_{\nu,\nu'} T_{\nu\nu'}(\boldsymbol{\tau}) f_{\nu\mathbf{l}+\boldsymbol{\tau}}^\dagger f_{\nu'\mathbf{l}}. \tag{42}$$

The (4×4)-matrices $T_{\nu\nu'}(\boldsymbol{\tau})$ are related to the $M_{ij}(\boldsymbol{\tau})$ by a rotation

$$T_{\nu\nu'}(\boldsymbol{\tau}) = -t \sum_{ij} \beta_{\nu i} M_{ij}(\boldsymbol{\tau}) \beta_{\nu' j}, \tag{43}$$

because $\left(\beta^{-1}\right)_{j\nu'} = \beta_{\nu' j}$. Finally, by collecting the contributions (39–42), we obtain an effective 'multi-orbital' Hubbard-like Hamiltonian

$$H_{t-V} = H_t^{(intra)} + H_V^{(intra)} + H_t^{(inter)} + H_{V,MF}^{(inter)}. \tag{44}$$

The effective Hamiltonian (44) has a lower symmetry compared to that of the original Hamiltonian (1). This may lead to an artificial low-symmetry ground-state solution, for instance, to a long-range charge/bond ordering. Here we suggest, however, that the geometrical frustration of the checkerboard lattice prevents this kind of long-range ordering, as was discussed already in the beginning of this section. Therefore we supplement the effective Hamiltonian (44) with additional restrictions, which prevent an artificial low-symmetry solution of (44). We require: (a) a homogeneous electron distribution over the lattice sites, $\left\langle c_i^\dagger c_i \right\rangle = n$, with n being the electron concentration, and (b) a bond-independence of hopping amplitudes, $\left\langle c_i^\dagger c_j \right\rangle = k$, where a pair of sites i, j denotes a bond (there are six bonds within each plaquette). Note that k is a real n-dependent quantity to be calculated self-consistently. On general grounds, one expects that $k > 0$ in a metallic phase and $k = 0$ in an insulating phase. Both requirements (a) and (b) together impose restrictions on cluster 'orbital' averages

$$\left\langle f_{\nu\mathbf{l}}^\dagger f_{\nu'\mathbf{l}} \right\rangle = \sum_{ij} \beta_{\nu i}\beta_{\nu' j} \left\langle c_{i\mathbf{l}}^\dagger c_{j\mathbf{l}} \right\rangle = n \sum_i \beta_{\nu i}\beta_{\nu' i} + k \left[\left(\sum_i \beta_{\nu i} \right) \left(\sum_j \beta_{\nu' j} \right) - \sum_i \beta_{\nu i}\beta_{\nu' i} \right]. \quad (45)$$

By using that $\sum_i \beta_{\nu i}\beta_{\nu' i} = \delta_{\nu\nu'}$ and

$$\sum_i \beta_{\nu i} = \left\{ \begin{array}{ll} 2; & \nu = 1 \\ 0; & \nu = 2,3,4 \end{array} \right\} \quad (46)$$

one obtains for $\nu = \nu'$ the following relations for cluster 'orbital' occupancies

$$\left\langle f_{1\mathbf{l}}^\dagger f_{1\mathbf{l}} \right\rangle = n+3k, \ (\nu = 1); \ \left\langle f_{\nu\mathbf{l}}^\dagger f_{\nu\mathbf{l}} \right\rangle = n-k, \ (\nu = 2,3,4). \quad (47)$$

If $\nu \neq \nu'$, the expression (45) leads to

$$\left\langle f_{\nu\mathbf{l}}^\dagger f_{\nu'\mathbf{l}} \right\rangle = 0, \ \ (\nu \neq \nu'). \quad (48)$$

For an isolated cluster with an integer electron occupancy equation (48) is obviously fulfilled because of symmetry arguments.

Based on the effective model (44) we calculate the electronic band structure from the Fourier transformation $G_{\nu\nu'}(\mathbf{q},\omega)$ of the retarded matrix Green's function:

$$G_{\nu\nu'}(\mathbf{l}-\mathbf{l}', t-t') = \left\langle \left\langle f_{\nu\mathbf{l}}(t) \,|f_{\nu'\mathbf{l}'}^\dagger(t') \right\rangle \right\rangle = -i\theta(t-t') \left\langle \{ f_{\nu\mathbf{l}}(t), f_{\nu'\mathbf{l}'}^\dagger(t') \} \right\rangle. \quad (49)$$

To obtain the equation of motion for $G_{\nu\nu'}(\mathbf{q},\omega)$, we use the method [27] of the two-time 'irreducible' Green's function. A successive differentiation of (49) with respect to both times t and t' with the use of properly defined projection procedure lead to the Dyson's equation:

$$\left[\omega\widehat{1} - \widehat{\Omega}(\mathbf{q}) - \widehat{\Sigma}(\mathbf{q},\omega) \right] \widehat{G}(\mathbf{q},\omega) = \widehat{1}. \quad (50)$$

Here $\widehat{1}$, $\widehat{\Omega}(\mathbf{q})$ and $\widehat{\Sigma}(\mathbf{q},\omega)$ are the unit, a frequency and a self-energy (4×4)-matrices, respectively. To define $\widehat{\Omega}$ and $\widehat{\Sigma}$ explicitly, it is convenient to introduce a notion of a scalar product of two fermionic operators A and B as $\langle A|B^\dagger \rangle = \langle \{A, B^\dagger\} \rangle$. In this notation, the matrix elements of $\widehat{\Omega}$ are

$$\Omega_{\nu\nu'}(\mathbf{q}) = \left\langle i\dot{f}_{\nu\mathbf{q}} | f_{\nu'\mathbf{q}}^\dagger \right\rangle = \left\langle \{ [f_{\nu\mathbf{q}}, H_{t-V}], f_{\nu'\mathbf{q}}^\dagger \} \right\rangle, \quad (51)$$

resulting in

$$\Omega_{\nu\nu'}(\mathbf{q}) = \delta_{\nu\nu'} E_\nu^{(1)} + T_{\nu\nu'}(\mathbf{q}) + \delta_{\nu\nu'} V \left(\sum_{\nu_1 (\neq \nu)} \langle n_{\nu_1} \rangle + \frac{3}{4} \langle N_c \rangle \right). \quad (52)$$

Here the $E_\nu^{(1)}$ are given by (36) and

$$T_{\nu\nu'}(\mathbf{q}) = \sum_{\{\boldsymbol{\tau}\}} e^{i\mathbf{q}\cdot\boldsymbol{\tau}} \ T_{\nu\nu'}(\boldsymbol{\tau}). \quad (53)$$

The frequency matrix $\widehat{\Omega}$ provides for a mean-field description of the electronic band structure. In order to include effects of electron correlations, the self-energy part $\widehat{\Sigma}$ must be calculated.

For this purpose, the set of basis operators $f_{\nu\mathbf{q}}$ is complemented with a new set of operators $F_{\nu\mathbf{q}}$ $(\nu = 1, ..., 4)$:

$$F_{\nu\mathbf{q}} = i\,\dot{f}_{\nu\mathbf{q}} - \sum_{\nu'} \Omega_{\nu\nu'}(\mathbf{q}) f_{\nu'\mathbf{q}}, \quad (54)$$

which are orthogonal to $f_{\nu\mathbf{q}}$, i.e. $\left\langle F_{\nu\mathbf{q}} | f_{\nu'\mathbf{q}'}^\dagger \right\rangle = 0$. Then, the self-energy $\widehat{\Sigma}$ has the form of an 'irreducible' matrix Green's function [27] whose elements are defined by

$$\Sigma_{\nu\nu'}(\mathbf{q},\omega) = \left\langle \left\langle F_{\nu\mathbf{q}} | F_{\nu'\mathbf{q}}^\dagger \right\rangle \right\rangle_\omega^{(irr)} = \left\langle \left\langle F_{\nu\mathbf{q}} | F_{\nu'\mathbf{q}}^\dagger \right\rangle \right\rangle_\omega - \sum_{\nu_1\nu_2} \left\langle \left\langle F_{\nu\mathbf{q}} | f_{\nu_1\mathbf{q}}^\dagger \right\rangle \right\rangle_\omega \frac{1}{\left\langle \left\langle f_{\nu_1\mathbf{q}} | f_{\nu_2\mathbf{q}}^\dagger \right\rangle \right\rangle_\omega} \left\langle \left\langle f_{\nu_2\mathbf{q}} | F_{\nu'\mathbf{q}}^\dagger \right\rangle \right\rangle_\omega. \quad (55)$$

The irreducible Green's function matrix $\left\langle \left\langle F_{\nu\mathbf{q}} | F_{\nu'\mathbf{q}}^\dagger \right\rangle \right\rangle_\omega^{(irr)}$ obeys the following equation (the lower indices are omitted for brevity):

$$\omega \left\langle \left\langle F | F^\dagger \right\rangle \right\rangle_\omega^{(irr)} = \left\langle F | F^\dagger \right\rangle + \left\{ \left\langle i\,\dot{F} \,| F^\dagger \right\rangle + \left\langle \left\langle i\,\dot{F} \,| -i\,\dot{F}^\dagger \right\rangle \right\rangle_\omega^{(irr)} \right\} \times \frac{1}{\langle F | F^\dagger \rangle} \left\langle \left\langle F | F^\dagger \right\rangle \right\rangle_\omega^{(irr)}. \quad (56)$$

We truncate this equation by neglecting in (56) the next-order 'irreducible' matrix Green's function $\left\langle\left\langle i\,\dot{F}\mid -i\,\dot{F}^{\dagger}\right\rangle\right\rangle_{\omega}^{(irr)}$. For the effective 'multiorbital' model (44), the truncation corresponds to the first step of the Hubbard-I approximation and results in the following form of $\widehat{\Sigma}$:

$$\Sigma_{\nu\nu'}(\mathbf{q},\omega)=\left[\omega\widehat{1}-\widehat{\Lambda}(\mathbf{q})\right]^{-1}_{\nu\nu'}\left\langle F_{\nu'\mathbf{q}}|F^{\dagger}_{\nu'\mathbf{q}}\right\rangle, \tag{57}$$

where the frequency matrix $\widehat{\Lambda}(\mathbf{q})$ is given by

$$\Lambda_{\nu\nu'}(\mathbf{q})=\frac{\left\langle i\,\dot{F}_{\nu\mathbf{q}}\,|F^{\dagger}_{\nu'\mathbf{q}}\right\rangle}{\left\langle F_{\nu'\mathbf{q}}|F^{\dagger}_{\nu'\mathbf{q}}\right\rangle}. \tag{58}$$

In the Hubbard-I approximation applied to the standard Hubbard model, the corresponding self-energy is $\mathbf{q}$-independent. We shall apply a similar approximation here by dropping the intercluster hopping term $H_t^{(inter)}$ which appears in the equation $i\,\dot{F}_{\nu\mathbf{q}}=[F_{\nu\mathbf{q}},H_{t-V}]$. In the following, $\widehat{\Lambda}$ and $\widehat{\Sigma}$ are $\mathbf{q}$-independent matrices and the latter is of the form

$$\Sigma_{\nu\nu'}(\omega)=\delta_{\nu\nu'}\frac{\left\langle F_{\nu\mathbf{l}}|F^{\dagger}_{\nu\mathbf{l}}\right\rangle}{\omega-\left\langle i\,\dot{F}_{\nu\mathbf{l}}\,|F^{\dagger}_{\nu\mathbf{l}}\right\rangle/\left\langle F_{\nu\mathbf{l}}|F^{\dagger}_{\nu\mathbf{l}}\right\rangle}. \tag{59}$$

With the definition (54), one obtains explicitly

$$F_{\nu\mathbf{l}}=V\delta N^{\nu}_{\mathbf{l}}f_{\nu\mathbf{l}}, \tag{60}$$

where

$$\delta N^{\nu}_{\mathbf{l}}=N^{\nu}_{\mathbf{l}}-\langle N^{\nu}_{\mathbf{l}}\rangle,\quad N^{\nu}_{\mathbf{l}}=N_{\mathbf{l}}-n_{\nu\mathbf{l}}=\sum_{\nu_1(\neq\nu)}n_{\nu_1\mathbf{l}}. \tag{61}$$

Then the diagonal elements of the frequency matrix entering into the denominator of (59) are found to be

$$\Lambda_{\nu\nu}=\frac{\left\langle i\,\dot{F}_{\nu\mathbf{l}}\,|F^{\dagger}_{\nu\mathbf{l}}\right\rangle}{\left\langle F_{\nu\mathbf{l}}|F^{\dagger}_{\nu\mathbf{l}}\right\rangle}=E^{(1)}_{\nu}+\frac{3}{4}V\langle N_c\rangle+V\frac{\left\langle N^{\nu}_{\mathbf{l}}\left(\delta N^{\nu}_{\mathbf{l}}\right)^2\right\rangle}{\left\langle\left(\delta N^{\nu}_{\mathbf{l}}\right)^2\right\rangle}. \tag{62}$$

Both averages, $\left\langle\left(\delta N^{\nu}_{\mathbf{l}}\right)^2\right\rangle$ and $\left\langle N^{\nu}_{\mathbf{l}}\left(\delta N^{\nu}_{\mathbf{l}}\right)^2\right\rangle$, are approximated in a mean-field manner. For instance, in this approximation, the mean value $\left\langle\left(\delta N^{\nu}_{\mathbf{l}}\right)^2\right\rangle$ which describes the intracluster charge correlations, reads

$$\left\langle\left(\delta N_{\mathbf{l}}\right)^2\right\rangle=\sum_{\nu_1(\neq\nu)}\langle n_{\nu_1\mathbf{l}}\rangle\left(1-\langle n_{\nu_1\mathbf{l}}\rangle\right).$$

We summarize the results for the self-energy as follow ($\langle n_{\nu\mathbf{l}}\rangle=\langle n_{\nu}\rangle$):

$$\Sigma_{\nu\nu}(\omega)=\frac{\sum_{\nu_1(\neq\nu)}\langle n_{\nu_1}\rangle\left(1-\langle n_{\nu_1}\rangle\right)}{\omega-\Lambda_{\nu\nu}}, \tag{63}$$

$$\Lambda_{\nu\nu}(\omega)=E^{(1)}_{\nu}+\frac{3}{4}V\langle N_c\rangle+V\frac{\sum_{\nu_1(\neq\nu)}\langle n_{\nu_1}\rangle\left(1-\langle n_{\nu_1}\rangle\right)^2}{\sum_{\nu_1(\neq\nu)}\langle n_{\nu_1}\rangle\left(1-\langle n_{\nu_1}\rangle\right)}+V\frac{\sum_{\nu_1(\neq\nu)}\sum_{\nu_2(\neq\nu,\nu_1)}\langle n_{\nu_1}\rangle\left(1-\langle n_{\nu_1}\rangle\right)\langle n_{\nu_2}\rangle}{\sum_{\nu_1(\neq\nu)}\langle n_{\nu_1}\rangle\left(1-\langle n_{\nu_1}\rangle\right)}. \tag{64}$$

In this expression the second term is the inter-cluster Hartree-Fock correction. The third and fourth terms are intra-cluster Hubbard-I type correlation corrections, where the latter appears only for the present 'multiorbital' Hubbard Hamiltonian. In the common Hubbard model (with just one 'orbital') only the third correction would be present. To perform self-consistent band-structure calculations, a chemical potential μ is introduced in a standard way. For a given spinless-fermion concentration n_0 varying within the range $0\leq n_0\leq 1$, the value of μ is determined from the equation

$$n_0=\frac{1}{4}\langle N_c\rangle=\frac{1}{4}\sum_{\nu=1}^{4}\langle n_{\nu}\rangle, \tag{65}$$

where $\langle n_{\nu}\rangle$ is an average 'orbital' cluster occupancy

$$\langle n_{\nu}\rangle=\frac{1}{M}\sum_{\mathbf{q}}\int_{-\infty}^{\mu}d\omega\,(-1/\pi)\,\mathrm{Im}\,G_{\nu\nu}(\mathbf{q},\omega). \tag{66}$$

Here the summation is over $M=N/4$ $\mathbf{q}$-vectors in the first Brillouin zone of the square lattice formed by the basic clusters in the checkerboard lattice. The 'orbital' occupancies should obey the relations (47).

The most representative results of the self-consistent band structure calculations are shown in Figures 6 and 7. In Figure 6, band spectra for different values of coupling V are given along highly symmetrical directions in the square Brillouin zone. To show the insulating gap opening in the band spectrum with increasing V, the electron concentration $n_0=1/2$ corresponding to an integer mean cluster occupancy $\langle N_c\rangle=2$ is chosen; the chemical potential μ is located at zero energy. From the upper panel, a doubly degenerate completely flat branch on the top of two highly dispersive bands is seen for the non-interacting case, $V=0$. For finite coupling V, but less than some critical value $V<V_c$, these four branches are split and the chemical potential intersects one of the dispersive branches as shown in the middle panel of Figure 6. In this weakly correlated regime of the model one expects a metallic state of the system. We found that starting from $V=V_c\approx 4t$, the spectrum is clearly split into the low- and high-energy Hubbard subbands separated with a gap growing as V increases above V_c. For a given concentration $\langle N_c\rangle=2$ and $V>V_c$, the four lowest Hubbard subbands

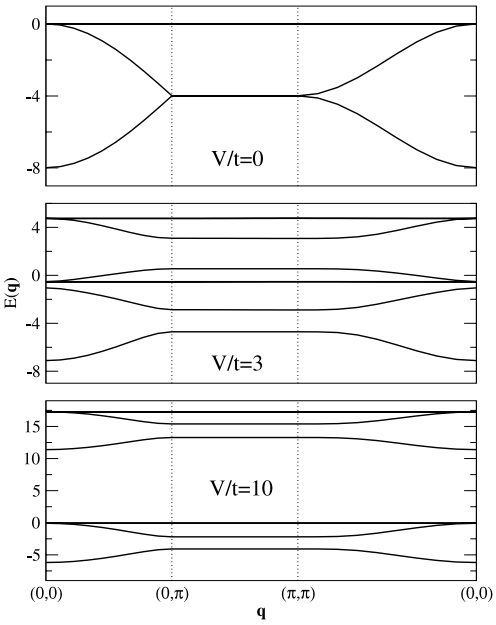

Fig. 6. Energy bands of spinless fermions on the checkerboard lattice calculated in the cluster approach for different values of inter-site repulsion $V/t = 0, 3 < V_c/t$ and $V/t = 10 > V_c/t \simeq 4$. The bands are unfolded along the highly symmetrical directions in the square Brillouin zone; energy unit is t $\equiv 1$. The electron concentration is chosen as $n = \frac{1}{2}$ (equivalent to $\langle N_c \rangle$ =2) and the chemical potential μ is fixed at zero energy.

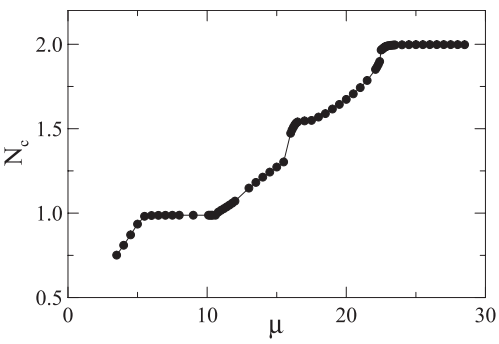

Fig. 7. Mean cluster occupancy $\langle N_c \rangle$ calculated as a function of the chemical potential μ at $V/t = 10$. Two wide flat regions with $d\langle N_c \rangle / d\mu = 0$ at $\langle N_c \rangle = 1, 2$ indicate an insulating state of the system.

are filled completely and located below the chemical potential μ as shown for $V = 10$ in the lower panel of Figure 6. If one includes a weak next neighbor hopping t', the former flat energy branches acquire a small dispersion, the picture of the insulating gap opening still retains at slightly changed value of the critical coupling V_c.

In this paper, however, we restrict ourselves to the study of the limit, t'=0. In this limit, to avoid discussing a rather special case of the partially filled upper flat band, the electron concentration is chosen to vary in the range $n_0 \leq 1/2$. Within this range, for strong coupling V the model displays an insulating state at the integer cluster occupancy $\langle N_c \rangle = 1$ as well. This can be easily seen from Figure 7, where the calculated mean cluster occupancy $\langle N_c \rangle$ is depicted as a function of the chemical potential μ for $V = 10$. The charge compressibility $d\langle N_c \rangle / d\mu$ is found to be zero in a wide range of varying μ at both integer occupancies $\langle N_c \rangle = 1, 2$. Near the occupancy value $\langle N_c \rangle = 1.5$, the sharp change of $\langle N_c \rangle$ is connected to the fact that μ intersects the flat band peculiarity in the density of states.

4 Conclusion

In this work we have studied an extended Hubbard type spinless fermion model for the frustrated checkerboard lattice which is a 2D analogue for pyrochlore or spinel-type lattices. We have studied the possibility of a metal-insulator phase transition as function of the inter-site Coulomb interaction and the band filling. We have used single-site and cluster representations of the model. In the latter the intra-cluster correlations are accounted for exactly by transforming to a 'cluster orbital' basis. Within a Green's function approach decouplings on Hartree-Fock and 'Hubbard-I' type level for the inter-site Coulomb term have been employed. In both approaches we find a metal-insulator transition for increasing V for half filling (that is one fermion per two sites) and in the cluster approach even for quarter filling. The MI transition is of the Mott Hubbard-type and is associated with a gap opening in the quasiparticle excitations. The critical interaction for the MI transition is $V_{c1}/t = 4.86$ in the single site approach and $V_c/t \simeq 4$ in the cluster approach are in reasonable agreement. We also consider the possibility of charge ordering within the single-site approach where we find a transition to a staggered CO state with $\mathbf{Q} = (\mathbf{0}, \mathbf{0})$ at $V_{c2}/t = 6.47$. This state may be a result of the approximations employed since for $V/t \to \infty$ CO has to vanish due to the macroscopic degeneracy of the ground state. Stabilisation of CO may indeed require the coupling to the lattice to lift this degeneracy [6]. This would imply the introduction of a deformation potential coupling of the relevant symmetry strain to spinless fermions and its corresponding elastic energy as was proposed in [6]. This extended model can still be treated within the Hubbard I-approximation using the method of Section 2. Further progress in understanding the nature of the insulating state caused by the *inter-site* Coulomb interaction may require the use of more advanced methods like cluster dynamical mean field methods which has so far not been achieved.

The authors are grateful to Prof. P. Fulde for suggesting the subject of studies and valuable discussions and comments.

References

1. M. Imada, A. Fujimori, Y. Tokura, Rev. Mod. Phys. **70**, 1039 (1998)
2. E. Wigner, Trans. Faraday Soc. **34**, 678 (1938)

3. E.J.W. Verwey, Nature (London) **144**, 327 (1939)
4. P.W. Anderson, Phys. Rev. **102**, 1008 (1956)
5. K. Matsuno, T. Katsufuji, S. Mori, M. Nohara, A. Machida, Y. Moritomo, K. Kato, E. Nishibori, M. Takata, M. Sakata, K. Kitazawa, H. Takagi, Phys. Rev. Lett. **90**, 096404 (2003)
6. Y.Z. Zhang, P. Fulde, P. Thalmeier, A. Yaresko, `cond-mat/0501408`; to be published in J. Phys. Soc. Jpn
7. K. Takada, H. Hidaka, H. Kotegawa, T.C. Kobayashi, K. Shimizu, H. Harima, K. Fujiwara, K. Miyoshi, J. Takeuchi, Y. Ohishi, T. Adachi, M. Takata, E. Nishibori, M. Sakata, T. Watanuki, O. Shimomura, in press; H. Ueda, C. Urano, M. Nohara, H. Takagi, K. Kitazawa, N. Takesita, N. Mori, unpublished; H. Takagi, *Proceed. American Phys. Soc., March Meeting 2003*
8. S. Kondo et al., Phys. Rev. Lett. **78**, 3729 (1997)
9. C. Urano et al., Phys. Rev. Lett. **85**, 1052 (2000)
10. Proceedings of the conference on 'Highly Frustrated Magnetism 2003', 26-30th August 2003, Grenoble, France; Special Issue J. Phys.: Condens. Matter 16, No. 11 (2004)
11. P. Fulde, K. Penc, N. Shannon, Annalen der Physik **11**, 892 (2002)
12. S. Fujimoto, Phys. Rev. Lett. **89**, 226402 (2002); S. Fujimoto, Phys. Rev. B **67**, 235102 (2003)
13. E. Runge, P. Fulde, Phys. Rev. B **70**, 245113 (2004)
14. K. Penc, F. Mila, Phys. Rev. B **49**, 9670 (1994)
15. Y.Z. Zhang, Phys. Rev. Lett. **92**, 246404 (2004)
16. M. Vojta, A. Huebsch, R.M. Noack, Phys. Rev. B **63**, 045105 (2001)
17. Y. Zhang, J. Callaway, Phys. Rev. B **39**, 9397 (1989); B. Chattopadhyay, D.M. Gaitonde, Phys. Rev. B **55**, 15364 (1997)
18. R. Pietig, R. Bulla, S. Blawid, Phys. Rev. Lett. **82**, 4046 (1999)
19. P.G.J. van Dongen, Phys. Rev. B **49**, 7904 (1994); P.G.J. van Dongen, Phys. Rev. B **50**, 14016 (1994)
20. J.R. Cullen, E. Callen, Phys. Rev. Lett. **26**, 236 (1971); V.I. Anisimov, I.S. Elfimov, N. Hamada, K. Terakura, Phys. Rev. B **54**, 4387 (1996)
21. A.A. Ovchinnikov, Sov. Phys. JETP **37**, 176 (1973)
22. P. Donohue, M. Tsuchiizu, T. Giamarchi, Y. Suzumura, Phys. Rev. B **63**, 045121 (2001)
23. R.H. McKenzie, J. Merino, J.B. Marstin, O.P. Sushkov, Phys. Rev. B **64**, 085109 (2001)
24. J. Hubbard, Proc. R. Soc. London, Series. A **276**, 238 (1963)
25. E. Lieb, Phys. Rev. Lett. **18**, 692 (1967)
26. Note that the ground state at $V/t \to \infty$ is quite different from that at $V/t = 0$ although CO is absent in both cases. For example the expectation values of the nearest- and next-nearest-neighbor charge correlation are different
27. Yu. A. Tserkovnikov, Theor. Matem. Fiz. **7**, 250 (1971); Yu. A. Tserkovnikov, Theor. Matem. Fiz. **49**, 219 (1981)